

Observation of spin splitting torque in a collinear antiferromagnet RuO₂

H. Bai,^{1,†} L. Han,^{1,†} X. Y. Feng,^{2,†} Y. J. Zhou,¹ Q. Wang,¹ W. X. Zhu,¹ X. Z. Chen,¹ F. Pan,¹ X. L. Fan^{2,*} and C. Song^{1,*}

¹Key Laboratory of Advanced Materials, School of Materials Science and Engineering, Tsinghua University, Beijing 100084, China

²The Key Lab for Magnetism and Magnetic Materials of Ministry of Education, Lanzhou University, Lanzhou 730000, China

Current-induced spin torques provide efficient data writing approaches for magnetic memories. Recently, the spin splitting torque (SST) was theoretically predicted (R. González-Hernández *et al.* *Phys. Rev. Lett.* **126, 127701 (2021)), which combines advantages of conventional spin transfer torque (STT) and spin-orbit torque (SOT) as well as enables controllable spin polarization. Here we provide the experimental evidence of SST in collinear antiferromagnet RuO₂ films. The spin current direction is found to be correlated to the crystal orientation of RuO₂ and the spin polarization direction is dependent on (parallel to) the Néel vector. These features are quite characteristic for the predicted SST. Our finding not only present a new member for the spin torques besides traditional STT and SOT, but also proposes a promising spin source RuO₂ for spintronics.**

*fanxiaolong@lzu.edu.cn; songcheng@mail.tsinghua.edu.cn

†These authors contributed equally to this work.

Current-induced spin torques not only enrich fundamental physics, but also provide efficient data writing approach for magnetic memories. The discovery of spin transfer torque (STT) brings about electrical switching of ferromagnetism, giving rise to the non-volatile magnetic random-access memory (STT-MRAM) with high speed and low consumption [1–5]. The longitudinal spin polarized current for STT is odd under time reversal (\mathcal{T}) and has high spin torque efficiency, due to the strong nonrelativistic ferromagnetic exchange splitting [1, 2, 4]. In contrast, transversal spin current with \mathcal{T} -even can be generated via the relativistic spin Hall effect (SHE) or/and the Rashba effect [6–8], which decouples reading and writing paths in MRAM and improves the device endurance. The resultant spin-orbit torque (SOT) was extensively studied in the last decade for SOT-MRAM [9, 10].

Recently, a distinct spin splitting torque (SST) with the origin of nonrelativistic anisotropic spin band splitting was theoretically predicted in antiferromagnets [11–17]. In this scenario, transversal spin current with high spin torque efficiency is induced by the magnetic exchange splitting (\mathcal{T} -odd), which provides a unique opportunity to combine the advantages of STT and SOT. Meanwhile, SST shows the advantage of controllable spin polarization, which would expand the horizon of spin torque switching. For example, SST offers a different approach for generating out-of-plane spin polarization, and the efficiency is expected to be higher than other mechanisms relying on low crystal symmetry and magnetic ordering [18–21]. This is because the out-of-spin polarization is directly induced by the strong magnetic exchange interaction inherent to antiferromagnets rather than the relatively weak spin orbit interaction [12]. The experiments below demonstrate the SST effect in a collinear antiferromagnet RuO_2 , where the direction of spin current is correlated to the crystal

orientation and the spin polarization direction is dependent on the magnetic orientation, *i.e.*, Néel vector of RuO₂.

RuO₂ was commonly considered as a paramagnet, until the recent finding of itinerant antiferromagnetism, which can persist above 300 K and the Néel vector tends to be aligned along [001]-axis [22, 23]. The crystal and magnetic structure of RuO₂ is shown in Fig. 1(a). RuO₂ is a rutile oxide with the $P4_2/mnm$ space group, where Ru atoms occupy the center of oxygen octahedrons [24]. Consequently, Ru atoms suffer from octahedral crystal field, generating anisotropic electronic structure and elliptical Fermi surface [16], as shown in Fig. 1(b). Note that Ru atoms of opposite magnetic sublattices are surrounded by different directional oxygen octahedrons (with 90° rotation). Such a sublattice rotation in real space results in anisotropic spin band splitting in momentum space [Fig. 1(b)], ensuring RuO₂ an efficient spin splitter to generate spin current. Two typical configurations to generate spin current were proposed in Ref. [12]. For the (100)-oriented RuO₂ film, charge current applied along $[0\bar{1}0]$ -axis can induce a transversal \mathcal{T} -odd spin current flowing along [100] direction (out-of-plane), and the spin polarization direction is parallel to the Néel vector ([001]-axis), as illustrated in Fig. 1(c). Differently, for the (110)-oriented RuO₂ film, charge current applied along $[1\bar{1}0]$ -axis produces only spin polarized current, the transversal spin current is forbidden due to the crystal symmetry, as displayed in Fig. 1(d).

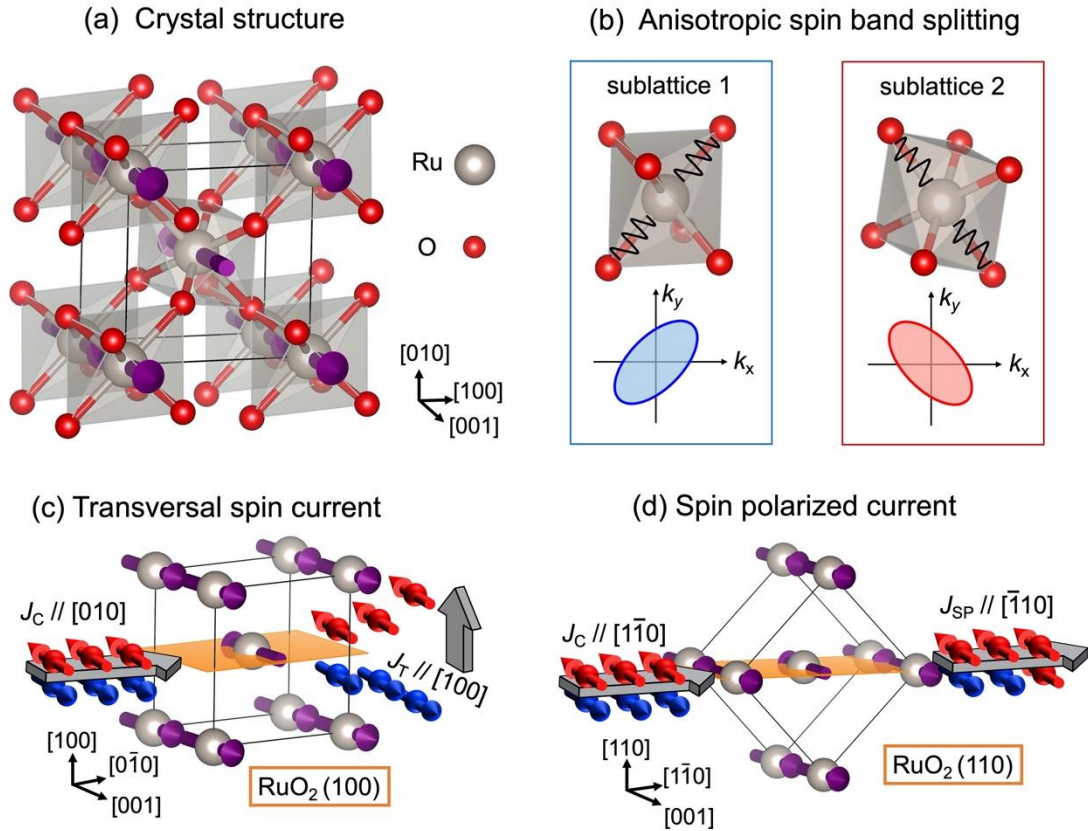


FIG. 1. (a) Crystal and magnetic structure of rutile RuO_2 . Grey and red spheres represent Ru and O atoms, respectively. Purple arrows mark the Ru local moments. (b) Schematic of anisotropic spin band splitting in RuO_2 . Oxygen octahedrons of two sublattices are rotated by 90° . The Ru atoms of two magnetic sublattices feel anisotropic octahedral crystal field, leading to anisotropic spin band splitting, as displayed by blue and red ellipses. (c) For the (100)-oriented RuO_2 film, transversal spin current (J_T) flowing along [100]-axis (out-of-plane) can be induced by the charge current along $[0\bar{1}0]$ -axis. The spin polarization is parallel to the Néel vector ([001]-axis). (d) For the (110)-oriented RuO_2 film, spin polarized current (J_{SP}) flowing along longitudinal direction can be generated by the charge current along $[1\bar{1}0]$ -axis. The spin polarization is parallel to the Néel vector.

To probe SST experimentally, we deposited (100)- and (110)-oriented RuO₂/Py bilayers onto YSZ(100) and MgO(100) substrates, and performed spin torque-ferromagnetic resonance (ST-FMR) measurements. It is expected to be observed: (i) spin torque efficiency of (100)-oriented RuO₂ film is larger than (110)-oriented RuO₂ film, the enhancement in RuO₂(100) is ascribed to SST, as illustrated in Fig. 1(c); (ii) spin polarization direction in (100)-oriented RuO₂ is correlated (parallel) to the Néel vector, e.g., spin polarization parallel (perpendicular) to the charge current is detected when charge current is applied parallel (perpendicular) to the Néel vector; (iii) the enhanced spin torque efficiency remains for the RuO₂(100)/Cu/Py sample, implying the bulk origin of SST.

For the analysis, ST-FMR spectrum can be decomposed by Eq. (1) into symmetric (V_S) and antisymmetric components (V_A), which respectively corresponds to in-plane and out-of-plane torques [25].

$$V(H) = V_S \frac{(\Delta H)^2}{(\Delta H)^2 + (H - H_{res})^2} + V_A \frac{\Delta H(H - H_{res})}{(\Delta H)^2 + (H - H_{res})^2} \quad (1)$$

where ΔH (H_{res}) parameters the line width (position) of resonance peak. The first (second) term is the symmetric (antisymmetric) line-shape with the amplitude of V_S (V_A). Effective spin Hall angle (θ_{SH}^{eff}) is used to evaluate the spin torque efficiency, which is expressed by [25]:

$$\theta_{SH}^{eff} = \frac{V_S}{V_A} \frac{e\mu_0 M_S t_{Py} t_{RuO_2}}{\hbar} \sqrt{1 + 4\pi M_{eff}/H_{res}} \quad (2)$$

where, μ_0 , M_S , $t_{py(RuO_2)}$ and $4\pi M_{eff}$ are permeability in vacuum, saturation magnetization of Py, thickness of Py and RuO₂ layers, and the demagnetization field, respectively. Angle-dependent ST-FMR measurement is used to distinguish the spin polarization direction, corresponding fitting formulas are shown below [21]:

$$V_S = V_{x,DL} \sin 2\varphi \sin \varphi + V_{y,DL} \sin 2\varphi \cos \varphi + V_{z,FL} \sin 2\varphi \quad (3)$$

$$V_A = V_{x,FL} \sin 2\varphi \sin \varphi + V_{y,FL} \sin 2\varphi \cos \varphi + V_{z,DL} \sin 2\varphi \quad (4)$$

Where, the $V_{i,FL(DL)}$ ($i = x, y, z$) is the rectified voltage induced by field-like (damping-like) torque of i -axis ($i = x, y, z$) polarized spins. φ represents the angle between radio frequency (rf) current and external magnetic field.

Figure 2 presents ST-FMR data in (100)- and (110)-oriented RuO₂/Py bilayers. For (100)-oriented RuO₂, both SST and SHE-induced SOT exist, thus a strong spin torque is expected to be detected, as illustrated in Fig. 2(a). Figure 2(b) shows the ST-FMR spectrum measured at $\varphi=45^\circ$. From the first glance, the amplitude of V_S is comparable to V_A , indicating the Py layer absorbs strong spin torque [25]. The situation turns out to be dramatically different for the (110)-oriented RuO₂, where SST vanishes and only the traditional SHE-induced SOT exists [Fig. 2(c)]. ST-FMR spectrum in Fig. 2(d) shows that the amplitude of V_S is much smaller than V_A , implying weak spin torques exert on the Py layer. The result is in a good agreement with our expectation due to the absence of SST in this scenario [Fig. 2(c)].

To quantitatively compare the spin torque efficiency of the two configurations, effective spin Hall angle θ_{SH}^{eff} is calculated by Eq. (2). Corresponding data are shown in Fig. 2(e). For both (100)- and (110)-oriented RuO₂, θ_{SH}^{eff} exhibits little variation as a function of microwave frequency, excluding artifacts rooted from the specified microwave frequency. The value of RuO₂(100) is $\theta_{SH}^{eff} \sim 0.08$, which is much larger than that of RuO₂(110) ~ 0.02 and is comparable to the SOT efficiency of the typical heavy metal Pt [25]. Furthermore, the effective spin Hall conductivity (σ_{SH}^{eff}) is also calculated for the two samples, where $\sigma_{SH}^{eff} = \theta_{SH}^{eff} / \rho_{xx}$. For the (100)-oriented RuO₂, σ_{SH}^{eff} is up to $5 \times 10^4 \hbar/2e \Omega^{-1} \text{ m}^{-1}$, which is around three times larger than that of the (110)-oriented RuO₂. The enhanced spin torque observed in

RuO₂(100)/Py bilayer can be ascribed to SST, coinciding with the theoretical prediction [12].

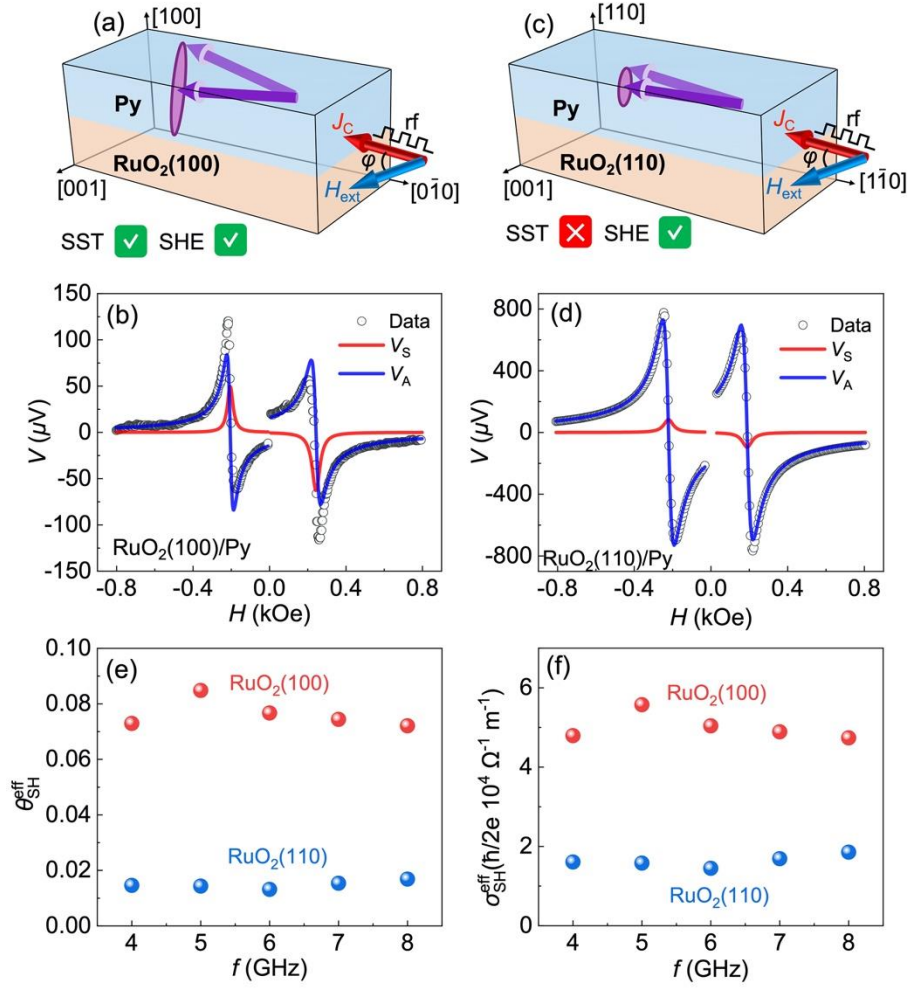


FIG. 2. ST-FMR measurements of (a) RuO₂(100)/Py and (c) RuO₂(110)/Py bilayers. For the (100)-oriented RuO₂, both SST and SHE-induced SOT exist, giving rise to strong spin torques. For the (110)-oriented RuO₂, SST is absent, only SHE-induced SOT contributes to the weak spin torques. The angle between charge current (J_C) and external magnetic field (H_{ext}) is termed as ϕ . (b, d) ST-FMR spectra of (b) RuO₂(100)/Py and (d) RuO₂(110)/Py bilayers measured at $\phi=45^\circ$. Circles are raw data; red and blue lines represent symmetric and antisymmetric voltages, respectively. (e, f) The calculated (e) spin torque efficiency θ_{SH}^{eff} and (f) effective spin Hall

conductivity σ_{SH}^{eff} at different microwave frequencies in (100)- and (110)-oriented RuO₂ films.

We now turn towards the dependence of spin polarization direction on the Néel vector of (100)-oriented RuO₂. Note that our RuO₂ films are in-plane multi-oriented, leading to inhomogeneous Néel vector directions, *i.e.*, multi-domain state. When charge current is applied along x -axis, the multi-directional Néel vectors enable spin current flowing along z -axis with spin polarizations along both x -axis (σ_x) and y -axis (σ_y), as depicted in Fig. 3(a). Magnetic field annealing was carried out in RuO₂(100)/Py bilayer to align the Néel vector along the direction of annealing field (H_{FA}). Subsequently, we carried out φ -dependent ST-FMR measurements for the scenario of charge current (J_C) perpendicular ($J_C \perp H_{FA}$) and parallel ($J_C // H_{FA}$) to the annealing field. It is expected that σ_y is the major term for $J_C \perp H_{FA}$, while σ_x is dominant for $J_C // H_{FA}$. The relative intensity of σ_x and σ_y is characterized by the ratio of spin torque efficiency $\theta_x^{eff}/\theta_y^{eff}$, which is proportional to the ratio of $V_{x,DL}/V_{y,DL}$.

Figure 3(b) and 3(c) show φ -dependent V_S for the configuration of $J_C \perp H_{FA}$ and $J_C // H_{FA}$, respectively. Note that the exchange bias effect could induce an extra signal with angular dependence different from our focused $V_{x,DL}$ ($\sim \sin 2\varphi \sin \varphi$) and $V_{y,DL}$ ($\sim \sin 2\varphi \cos \varphi$) [26], which was subtracting in Fig. 3(b) and 3(c). For the case of $J_C \perp H_{FA}$, the angular dependent signal can be fitted by $\sin 2\varphi \cos \varphi$ function, indicating the major contribution from σ_y , which is supported by the line-shape separation result that the amplitude of $V_{y,DL}$ (blue line) is much larger than that of $V_{x,DL}$ (red line). The ratio of $\theta_x^{eff}/\theta_y^{eff}$ in this case is ~ 0.07 . The scenario differs dramatically when $J_C // H_{FA}$. Concomitant data in Fig. 3(c) are not in consistent with the angular dependence

$\sim \sin 2\varphi \cos \varphi$. By the fitting based on Eq. (3), it is found that amplitude of $V_{x,DL}$ is comparable to that of $V_{y,DL}$ and the $\theta_x^{eff}/\theta_y^{eff}$ is ~ 0.84 , revealing that obvious σ_x emerges. This finding demonstrates the existence of SST in (100)-oriented RuO_2 , as analyzed above. In addition to two specific positions ($J_C \perp H_{FA}$ and $J_C // H_{FA}$), we plot in Fig. 3(d) the ratios of $\theta_x^{eff}/\theta_y^{eff}$ at different β , where β is the angle between J_C and H_{FA} in ST-FMR measurements. Here the $\theta_x^{eff}/\theta_y^{eff}$ ratios take the absolute value, which can be well fitted by $\cos\beta/(\sin\beta+C)$, and C is a constant. This result further supports the conclusion that spin polarization generated in $\text{RuO}_2(100)$ is dependent on (parallel to) the Néel vector, which is quite characteristic for SST as discussed in Figure 1(c).

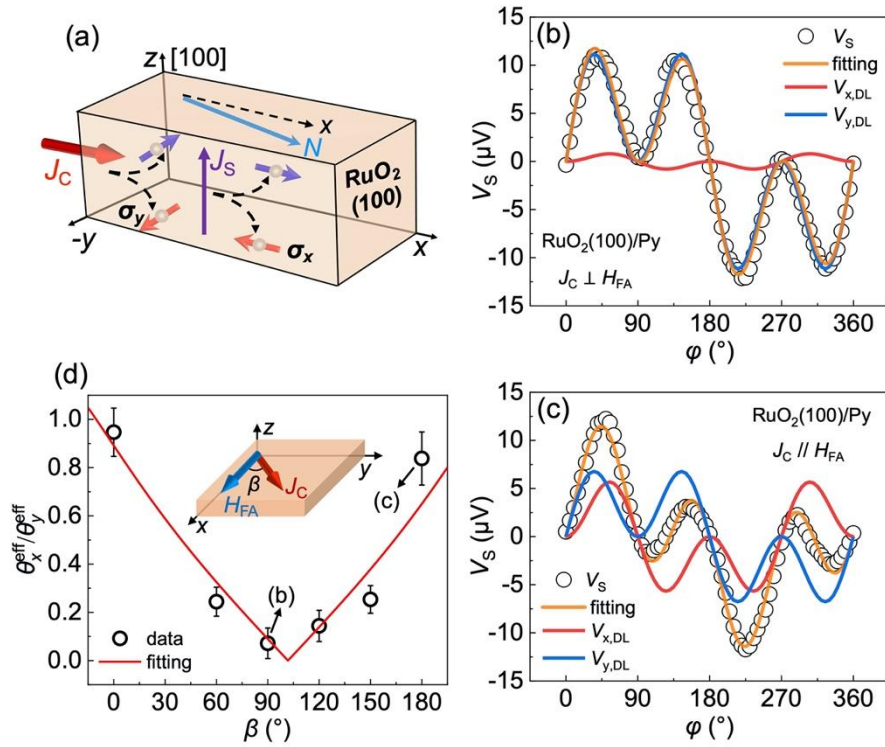


FIG. 3. (a) Schematic of transversal spin current generation in (100)-oriented RuO_2 . When charge current applied at tilted angle to the Néel vector, spin polarizations along both x-axis (σ_x) and y-axis (σ_y) can be generated and flow along the z-axis. (b, c) φ -dependent symmetric voltage (V_S) for configurations of current (b) perpendicular or

(c) parallel to the annealing field. Orange lines are the fitting result by Eq. (3). Red and blue lines represent damping-like torque contribution of σ_x and σ_y , respectively. (d) Ratios of $\theta_x^{eff}/\theta_y^{eff}$ as a function of β , where β is the angle between J_C and H_{FA} in ST-FMR measurements. Red line is fitted by the expression of $\cos\beta/(\sin\beta+C)$. The specific positions of $J_C \perp H_{FA}$ and $J_C // H_{FA}$ for $\beta = 90^\circ$ and 180° , respectively, are highlighted.

Besides SST, magnetic moment-dependent spin torque behaviors were also observed due to the magnetic (antiferromagnetic) spin Hall effect (MSHE or AFM-SHE), where the interfacial effect (*e.g.*, interfacial spin precession) is proposed to play a key role in these material systems [19, 21, 27–30]. Differently, direct magnetic exchange interaction is considered as the origin of the \mathcal{T} -odd SST, thus SST in RuO₂ possesses following characteristics in the contrast to MSHE or AFM-SHE: dominant bulk contribution, spin polarization parallel to the Néel vector and higher \mathcal{T} -odd spin torque efficiency. To demonstrate the major contribution of SST is from RuO₂ bulk, we show in Fig. 4 the ST-FMR data of (100)- and (110)-oriented RuO₂/Cu/Py samples. For this experiment, we focus on the dependence of Cu insertion on the magnitude of SST signals. A comparison of ST-FMR spectra displayed in Fig. 4(a) and 4(b) shows that the amplitude of the V_S signal is much larger in (100)-oriented RuO₂ sample than that of (110)-oriented one, indicating the spin torque efficiency of former is larger than that of the latter. Then we show the calculated θ_{SH}^{eff} at different frequencies in Fig. 4(c), which exhibits a weak dependence on microwave frequency for both samples. The value of RuO₂(100)/Cu/Py sample is ~ 0.06 , which is larger than that of RuO₂(110)/Cu/Py sample ~ 0.02 . The enhancement of spin torques in the RuO₂(100)/Cu/Py sample

demonstrates that RuO₂ bulk dominates the generation of SST. We point out that the slight reduction of θ_{SH}^{eff} compared to the counterpart without Cu insertion is reasonable because the additional interface and Cu spacer would increase the spin loss.

Besides the advantage of controllable spin polarization, SST in RuO₂ brings about its ultrahigh spin Hall conductivity, making it a promising spin source in spintronics. Combing the predicted ultrahigh charge-spin conversion efficiency [12] and ultralow resistivity measured in single crystal [31], the maximum σ_{SH}^{eff} of RuO₂(100) is as high as $8 \times 10^5 \hbar/2e \Omega^{-1} \text{ m}^{-1}$, which is larger than typical heavy metals and topological insulators, *e.g.*, Pt $\sim 3.4 \times 10^5$, β -Ta $\sim 8 \times 10^4$, Bi₂Se₃ $\sim 2 \times 10^5 \hbar/2e \Omega^{-1} \text{ m}^{-1}$ [7, 25, 32]. Such a large value is ascribed to the nonrelativistic spin splitting effect. In addition, some other interesting physical behaviors including crystal Hall effect [33, 34], giant tunneling magnetoresistance [35, 36] as well as strain-induced superconductivity [37] were theoretically predicted or experimental reported in rutile RuO₂. All these intriguing findings make RuO₂ an emergent material in condensed matter physics.

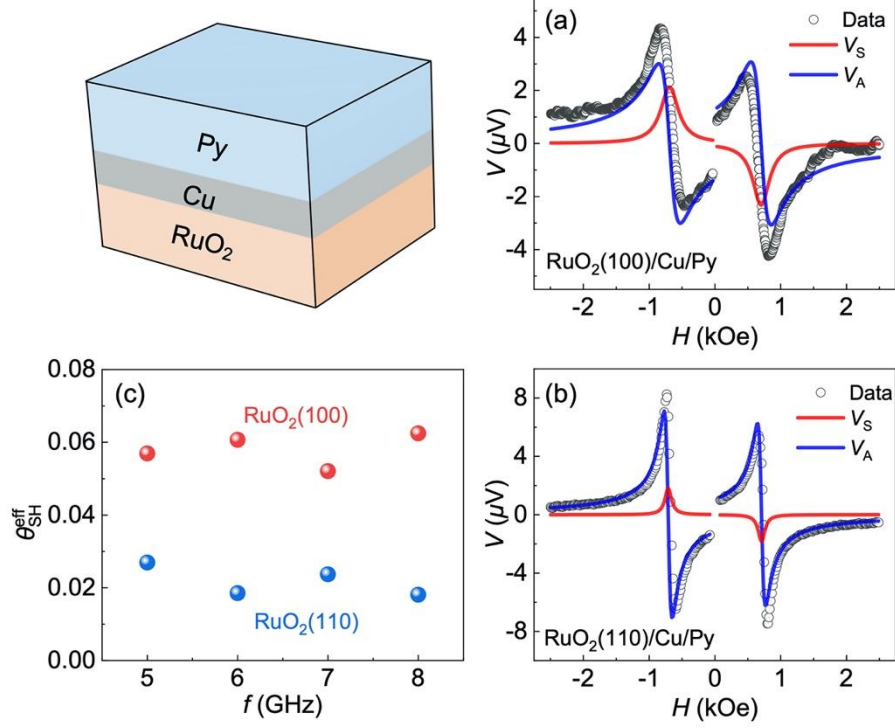


Fig. 4. ST-FMR measurement results for the samples with Cu insertion. ST-FMR spectra of (a) RuO₂(100)/Cu/Py and (b) RuO₂(110)/Cu/Py samples. Red and blue lines are symmetric (V_S) and antisymmetric (V_A) voltages. (c) Calculated θ_{SH}^{eff} at different microwave frequencies for RuO₂(100)/Cu/Py and RuO₂(110)/Cu/Py samples.

In summary, we provide experimental evidences for the observation of spin splitting torque in a collinear antiferromagnet RuO₂, where three typical features of SST were observed: (i) spin torque efficiency in RuO₂(100) film is larger than RuO₂(110) film, because of crystal orientation-dependent spin current flowing along [100]-axis of RuO₂; (ii) the spin polarization direction in RuO₂(100) is dependent on (parallel to) the Néel vector; (iii) spin torque efficiencies measured in RuO₂(100) samples with and without Cu insertion are comparable, revealing the bulk contribution is dominant. Spin splitting torque in RuO₂ brings about controllable spin polarization combined with ultrahigh spin Hall conductivity, which makes it a promising spin source in spintronics.

Note Added—After finishing the experimental work and during the manuscript preparation, we are aware of a relevant work that demonstrated (101)-oriented RuO₂ can generate out-of-plane spin polarization [38]. In this work, we mainly focus on the spin splitting torque generated in (100)-oriented RuO₂.

Reference

- [1] L. Berger, *Emission of Spin Waves by a Magnetic Multilayer Traversed by a Current*, Phys. Rev. B **54**, 9353 (1996).
- [2] J. C. Slonczewski, *Current-Driven Excitation of Magnetic Multilayers*, J. Magn. Magn. Mater. **159**, L1 (1996).
- [3] J. A. Katine, F. J. Albert, R. A. Buhrman, E. B. Myers, and D. C. Ralph, *Current-Driven Magnetization Reversal and Spin-Wave Excitations in Co/Cu/Co Pillars*, Phys. Rev. Lett. **84**, 3149 (2000).
- [4] A. Brataas, A. D. Kent, and H. Ohno, *Current-Induced Torques in Magnetic Materials*, Nat. Mater. **11**, 372 (2012).
- [5] D. Apalkov, A. Khvalkovskiy, S. Watts, V. Nikitin, X. Tang, D. Lottis, K. Moon, X. Luo, E. Chen, A. Ong, A. Driskill-Smith, and M. Krounbi, *Spin-Transfer Torque Magnetic Random Access Memory (STT-MRAM)*, ACM J. Emerg. Technol. Comput. Syst. **9**, 1 (2013).
- [6] I. M. Miron, K. Garello, G. Gaudin, P. J. Zermatten, M. V. Costache, S. Auffret, S. Bandiera, B. Rodmacq, A. Schuhl, and P. Gambardella, *Perpendicular Switching of a Single Ferromagnetic Layer Induced by In-Plane Current Injection*, Nature **476**, 189 (2011).

- [7] L. Liu, C. F. Pai, Y. Li, H. W. Tseng, D. C. Ralph, and R. A. Buhrman, *Spin-Torque Switching with the Giant Spin Hall Effect of Tantalum*, *Science* **336**, 555 (2012).
- [8] L. Liu, O. J. Lee, T. J. Gudmundsen, D. C. Ralph, and R. A. Buhrman, *Current-Induced Switching of Perpendicularly Magnetized Magnetic Layers Using Spin Torque from the Spin Hall Effect*, *Phys. Rev. Lett.* **109**, 096602 (2012).
- [9] A. Manchon, J. Železný, I. M. Miron, T. Jungwirth, J. Sinova, A. Thiaville, K. Garello, and P. Gambardella, *Current-Induced Spin-Orbit Torques in Ferromagnetic and Antiferromagnetic Systems*, *Rev. Mod. Phys.* **91**, 035004 (2019).
- [10] C. Song, R. Zhang, L. Liao, Y. Zhou, X. Zhou, R. Chen, Y. You, X. Chen, and F. Pan, *Spin-Orbit Torques: Materials, Mechanisms, Performances, and Potential Applications*, *Prog. Mater. Sci.* **118**, 100761 (2021).
- [11] M. Naka, S. Hayami, H. Kusunose, Y. Yanagi, Y. Motome, and H. Seo, *Spin Current Generation in Organic Antiferromagnets*, *Nat. Commun.* **10**, 4305 (2019).
- [12] R. González-Hernández, L. Šmejkal, K. Výborný, Y. Yahagi, J. Sinova, T. Jungwirth, and J. Železný, *Efficient Electrical Spin Splitter Based on Nonrelativistic Collinear Antiferromagnetism*, *Phys. Rev. Lett.* **126**, 127701 (2021).
- [13] M. Naka, Y. Motome, and H. Seo, *Perovskite as a Spin Current Generator*, *Phys. Rev. B* **103**, 125114 (2021).
- [14] K. H. Ahn, A. Hariki, K. W. Lee, and J. Kuneš, *Antiferromagnetism in RuO₂ as d-Wave Pomeranchuk Instability*, *Phys. Rev. B* **99**, 184432 (2019).

- [15] L. D. Yuan, Z. Wang, J. W. Luo, E. I. Rashba, and A. Zunger, *Giant Momentum-Dependent Spin Splitting in Centrosymmetric Low- Z Antiferromagnets*, Phys. Rev. B **102**, 014422 (2020).
- [16] S. Hayami, Y. Yanagi, and H. Kusunose, *Bottom-up Design of Spin-Split and Reshaped Electronic Band Structures in Antiferromagnets without Spin-Orbit Coupling: Procedure on the Basis of Augmented Multipoles*, Phys. Rev. B **102**, 144441 (2020).
- [17] L. D. Yuan, Z. Wang, J. W. Luo, and A. Zunger, *Strong Influence of Nonmagnetic Ligands on the Momentum-Dependent Spin Splitting in Antiferromagnets*, Phys. Rev. B **103**, 224410 (2021).
- [18] D. Macneill, G. M. Stiehl, M. H. D. Guimaraes, R. A. Buhrman, J. Park, and D. C. Ralph, *Control of Spin–Orbit Torques through Crystal Symmetry in WTe_2 /Ferromagnet Bilayers*, Nat. Phys. **13**, 300 (2017).
- [19] S. H. C. Baek, V. P. Amin, Y. W. Oh, G. Go, S. J. Lee, G. H. Lee, K. J. Kim, M. D. Stiles, B. G. Park, and K. J. Lee, *Spin Currents and Spin-Orbit Torques in Ferromagnetic Trilayers*, Nat. Mater. **17**, 509 (2018).
- [20] T. Nan, C. X. Quintela, J. Irwin, G. Gurung, D. F. Shao, J. Gibbons, N. Campbell, K. Song, S. Y. Choi, L. Guo, R. D. Johnson, P. Manuel, R. V. Chopdekar, I. Hallsteinsen, T. Tybell, P. J. Ryan, J. W. Kim, Y. Choi, P. G. Radaelli, D. C. Ralph, E. Y. Tsybal, M. S. Rzchowski, and C. B. Eom, *Controlling Spin Current Polarization through Non-Collinear Antiferromagnetism*, Nat. Commun. **11**, 4671 (2020).
- [21] X. Chen, S. Shi, G. Shi, X. Fan, C. Song, X. Zhou, H. Bai, L. Liao, Y. Zhou, H. Zhang, A. Li, Y. Chen, X. Han, S. Jiang, Z. Zhu, H. Wu, X. Wang, D. Xue, H.

- Yang, and F. Pan, *Observation of the Antiferromagnetic Spin Hall Effect*, Nat. Mater. **20**, 800 (2021).
- [22] T. Berlijn, P. C. Snijders, O. Delaire, H. D. Zhou, T. A. Maier, H. B. Cao, S. X. Chi, M. Matsuda, Y. Wang, M. R. Koehler, P. R. C. Kent, and H. H. Weitering, *Itinerant Antiferromagnetism in RuO₂*, Phys. Rev. Lett. **118**, 077201 (2017).
- [23] Z. H. Zhu, J. Stremper, R. R. Rao, C. A. Occhialini, J. Pellicciari, Y. Choi, T. Kawaguchi, H. You, J. F. Mitchell, Y. Shao-Horn, and R. Comin, *Anomalous Antiferromagnetism in Metallic RuO₂ Determined by Resonant X-Ray Scattering*, Phys. Rev. Lett. **122**, 017202 (2019).
- [24] L. F. Mattheiss, *Electronic Structure of RuO₂, OsO₂, and IrO₂*, Phys. Rev. B **13**, 2433 (1976).
- [25] L. Liu, T. Moriyama, D. C. Ralph, and R. A. Buhrman, *Spin-Torque Ferromagnetic Resonance Induced by the Spin Hall Effect*, Phys. Rev. Lett. **106**, 036601 (2011).
- [26] H. Saglam, J. C. Rojas-Sanchez, S. Petit, M. Hehn, W. Zhang, J. E. Pearson, S. Mangin, and A. Hoffmann, *Independence of Spin-Orbit Torques from the Exchange Bias Direction in Ni₈₁Fe₁₉/IrMn Bilayers*, Phys. Rev. B **98**, 094407 (2018).
- [27] M. Kimata, H. Chen, K. Kondou, S. Sugimoto, P. K. Muduli, M. Ikhlas, Y. Omori, T. Tomita, A. H. MacDonald, S. Nakatsuji, and Y. Otani, *Magnetic and Magnetic Inverse Spin Hall Effects in a Non-Collinear Antiferromagnet*, Nature **565**, 627 (2019).
- [28] A. Mook, R. R. Neumann, A. Johansson, J. Henk, and I. Mertig, *Origin of the Magnetic Spin Hall Effect: Spin Current Vorticity in the Fermi Sea*, Phys. Rev. Res. **2**, 023065 (2020).

- [29] V. P. Amin and M. D. Stiles, *Spin Transport at Interfaces with Spin-Orbit Coupling: Formalism*, Phys. Rev. B **94**, 104419 (2016).
- [30] V. P. Amin and M. D. Stiles, *Spin Transport at Interfaces with Spin-Orbit Coupling: Phenomenology*, Phys. Rev. B **94**, 104420 (2016).
- [31] W. D. Ryden, A. W. Lawson, and C. C. Sartain, *Electrical Transport Properties of IrO_2 and RuO_2* , Phys. Rev. B **1**, 1494 (1970).
- [32] A. R. Mellnik, J. S. Lee, A. Richardella, J. L. Grab, P. J. Mintun, M. H. Fischer, A. Vaezi, A. Manchon, E. A. Kim, N. Samarth, and D. C. Ralph, *Spin-Transfer Torque Generated by a Topological Insulator*, Nature **511**, 449 (2011).
- [33] L. Šmejkal, R. González-Hernández, T. Jungwirth, and J. Sinova, *Crystal Time-Reversal Symmetry Breaking and Spontaneous Hall Effect in Collinear Antiferromagnets*, Sci. Adv. **6**, eaaz8809 (2020).
- [34] Z. Feng, X. Zhou, L. Šmejkal, L. Wu, Z. Zhu, H. Guo, R. González-Hernández, X. Wang, H. Yan, P. Qin, X. Zhang, H. Wu, H. Chen, Z. Xia, C. Jiang, M. Coey, J. Sinova, T. Jungwirth, and Z. Liu, *Observation of the Crystal Hall Effect in a Collinear Antiferromagnet*, arXiv:2002.08712 (2021).
- [35] L. Šmejkal, A. H. MacDonald, J. Sinova, S. Nakatsuji, and T. Jungwirth, *Anomalous Hall Antiferromagnets*, arxiv:2107.03321 (2021).
- [36] D.-F. Shao, S.-H. Zhang, M. Li, and E. Y. Tsybal, *Spin-Neutral Currents for Spintronics*, arXiv:2013.09219 (2021).
- [37] M. Uchida, T. Nomoto, M. Musashi, R. Arita, and M. Kawasaki, *Superconductivity in Uniquely Strained RuO_2 Films*, Phys. Rev. Lett. **125**, 147001 (2020).

- [38] A. Bose, N. J. Schreiber, R. Jain, D. Shao, H. P. Nair, J. Sun, X. S. Zhang, D. A. Muller, E. Y. Tsybal, D. G. Schlom, and D. C. Ralph, *Tilted Spin Current Generated by the Collinear Antiferromagnet RuO₂*, arxiv:2108.09150 (2021).